

PURIFYING MK-STYX FOR X-RAY CRYSTALLOGRAPHY TO UNDERSTAND THE ROLE OF THIS PSEUDOPHOSPHATASE IN STRESS RESPONSE PATHWAYS

Emma Marie Wilber Hepworth
Department of Biology, College of William & Mary
Advisor: Shantá D. Hinton, Ph.D.

Abstract

The pseudophosphatase MK-STYX [MAPK (mitogen-activated protein kinase) - phosphoserine/threonine/tyrosine-binding protein] is an atypical MKP (MAPK phosphatase). MK-STYX consists of two domains, a DUSP domain (dual-specificity phosphatase) and CH2 domain (cell division cycle 25 phosphatase homology 2). The DUSP domain of MK-STYX lacks critical histidine and cysteine residues in the active site motif (HCX₅R), rendering it catalytically inactive. The CH2 domain, which is interrupted by a KIM (kinase interacting motif), lacks consecutive arginines required for its MKP active homologs to bind target proteins. Despite these mutations from its active homologs, MK-STYX is an important regulator of multiple pathways, including stress response, apoptosis, and neurite formation. Furthermore, MK-STYX has been implicated in various cancers, including liver cancer. Uncovering the macromolecular structure of MK-STYX is the key to understanding the function of MK-STYX, what role MK-STYX plays in signaling pathways, why it induces particular phenotypes, and how these traits differ from other MKPs. A critical step in obtaining the structure of MK-STYX through X-ray crystallography is purifying the protein in order to develop a protein crystal. Multiple methods of purification were analyzed to determine the one best suited to MK-STYX. These findings were then utilized to start a crystal screen to identify crystallization conditions.

Introduction

Communication is key to ensuring smooth operation within each cell. Nowadays,

people have many ways to communicate with their coworkers, friends, and family, to carry out projects, coordinate plans, and remain abreast of important events. Similarly, cells have numerous ways in which they “talk”, both within the cell and with others, through signaling pathways¹. One important messenger is the phosphate molecule, which when added (through phosphorylation) or removed (through dephosphorylation) from a protein can change the shape and function of that protein². The processes of phosphorylation and dephosphorylation, known as the phosphorylation cascade, are highly regulated within the cell to maintain homeostasis. Two kinds of proteins have the vital job of maintaining this delicate balance, kinases, which are responsible for phosphorylation, and phosphatases, which are responsible for dephosphorylation^{2,3}.

While enzymes such as kinases and phosphatases are essential to proper cell function, there are also proteins known as “pseudoenzymes” that play an important cellular role⁴. These proteins are catalytically inactive homologs of enzymes such as: kinases, phosphatases, proteases, synthetases, etc. Pseudoenzymes are highly conserved evolutionarily and an estimated 10% of the proteins encoded in the human genome are pseudoenzymes^{1,5,6}. However, their biologic role remains elusive. While these proteins were previously thought to be “dead” enzymes with no unique cellular functions, they have emerged as important signaling regulators over the last decade as researchers uncover new information that reveals a fascinating and complex area of study^{1,4,6-8}. One such protein of interest is the pseudophosphatase MK-

STYX [MAPK (mitogen-activated protein kinase)-phosphoserine/threonine/tyrosine-binding protein], also called DUSP-24 (dual-specificity protein phosphatase 24) or STYXL1 (serine/threonine/tyrosine-interacting-like protein 1)^{9–11}.

MK-STYX is a catalytically inactive PTP (protein tyrosine phosphatase) and the only catalytically inactive member of the mammalian MKP (MAPK phosphatase) subfamily of DUSPs (dual-specificity phosphatases)^{10–12}. The main function of MKPs is to dephosphorylate target kinases, MAPKs/ERKs (extracellular signal regulated kinases), in order to regulate MAPK/ERK signaling pathways^{13,14}. MKPs carry out this function using two conserved domains, an N-terminal noncatalytic binding domain and a C-terminal catalytic domain (DUSP domain) (Figure 1)^{13,15}. The N-terminal noncatalytic domain determines substrate specificity and is responsible for recognizing and binding the target MAPK/ERK^{13,14,16}. The C-terminal catalytic domain removes a phosphate group from the MAPK/ERK.



Figure 1: Schematic Representation of MK-STYX. Shows the arrangement of the N-terminal noncatalytic domain and the C-terminal catalytic domain, along with the location of key atypical regions within these domains. Image created with BioRender.

PTPs have a highly conserved signature active site motif consisting of histidine and cysteine, followed by any five amino acids, and an arginine (HCX₅R)^{3,17–19}. This is the region of the protein that catalyzes the removal of a phosphate from the substrate. However, the active site of MK-STYX has the sequence FSTQGISR (containing phenylalanine and serine), which lacks the critical histidine and cysteine residues and renders MK-STYX catalytically inactive (Table 1)^{1,10,11}. The inactive DUSP domain of MK-STYX is also referred to as a “STYX” domain, after the prototypical pseudophosphatase STYX

(serine/threonine/tyrosine-interacting protein), classifying MK-STYX as a “STYX” domain PTP^{20–22}.

In addition to an atypical C-terminal catalytic domain, MK-STYX has an atypical N-terminal domain (Figure 1)¹¹. Typical MKPs have an N-terminal noncatalytic domain composed of a CH2 domain (cell division cycle 25 phosphatase homology 2 domain) interrupted by a KIM (kinase-interacting motif)¹³. This noncatalytic domain is used for substrate recognition and docking of the target at the KIM, allowing the DUSP domain to then remove the phosphate group^{14,15,23}. However, compared to its active homologs, MK-STYX lacks a cluster of consecutive arginine residues in its KIM that are necessary to dock MAPKs/ERKs (Table 1)^{11,16,24}. This may explain why studies have found that MK-STYX does not bind MAPK/ERK or modulate MAPK/ERK1/2 signaling^{1,11,25–28}. Previously conducted computational studies also found that this difference in the KIM of MK-STYX is predicted to alter the shape of the associated binding pocket, possibly allowing MK-STYX to bind a novel set of substrates²⁴.

	KIM	Active Site Motif
Consensus Sequence	XIXLRRXKKG	HCXXXXXR
MKP-1	TIVRRRAK-G	HCQAGISR
MKP-3	GIMLRLQKG	HCLAGISR
MK-STYX	ITALRVKKKN	FSTQGISR

Table 1: Table Comparing the Sequences of MK-STYX and its Active Homologs. Lists the critical sequences within the KIM and active site motif of MK-STYX with those of its active homologs, MKP-1 (DUSP-1) and MKP-3 (DUSP-6)^{11,23,31}.

Given that the domains of MK-STYX have been reported to lack the conserved functions of its active homologs, it would be easy to assume that MK-STYX has lost its overall protein function. However, while MK-STYX may not function in the same way as a canonical MKP, it is very much still a functioning protein with an important role in cellular pathways. In previous studies, MK-STYX has demonstrated the ability to regulate

apoptosis pathways, stress granule formation, neurite formation, and has been implicated as a promoter of oncogenesis and malignancy in glioma and hepatocellular carcinoma^{1,10,11,25,26,29-33}.

Perhaps the role of MK-STYX that is best characterized, is its role in stress response pathways. MK-STYX is a regulator of apoptotic signaling by inducing stress-activated mitochondrial-dependent apoptosis by inhibiting the phosphatase PTPM1 (PTP localized to the mitochondrion 1)^{1,11,25,29}. Another critical role of MK-STYX in the cellular stress response is the ability of MK-STYX to reduce stress granules (SGs), membraneless organelles that form in the cytosol as a protective response to stressful physiologic conditions^{10,34-37}. SGs are untranslated messenger ribonucleoproteins (mRNPs) that are stalled in the translation initiation stage of protein synthesis. While SGs are a protective response to stressful cellular conditions, SGs that persist in the cytosol, instead of being properly cleared, become toxic. Prolonged SGs are linked to neurodegenerative diseases and certain cancers^{32,34,35}. The physiologic conditions that induce SGs can be both physical and chemical, including thermal stress, osmotic stress, and oxidative stress, the latter of which can be induced by a variety of factors such as sodium arsenate and even microgravity³⁷⁻⁴¹.

The catalytic activity of MK-STYX can be experimentally restored by replacing phenylalanine (position 245) and serine (position 246) with histidine and cysteine residues, respectively, to create a catalytically active mutant (MK-STYX_{active mutant})^{10,42}. With the PTP active site motif (HCX₅R) restored, MK-STYX_{active mutant} regains phosphatase activity and is expected to maintain the fold and substrate binding capabilities of MK-STYX^{1,10,11,24,42}. However, MK-STYX_{active mutant} does not reduce SGs, both those induced by G3BP-1 (Ras-GTPase-activating protein SH3 domain-binding protein-1) and

endogenous SGs^{1,10}. Actually, the opposite effect is seen and MK-STYX_{active mutant} increases the size of G3BP-1-induced SGs.

The mechanisms used by MK-STYX to induce these effects are not well understood, and so characterizing the mechanisms and function of MK-STYX is of utmost importance in order to understand its role in maintaining proper cell function and how it is involved in different diseases.

Objectives

1. Determine the function of the domains in MK-STYX and how they interact.
2. Uncover the novel mode of action utilized by MK-STYX in signaling pathways by comparing the structure of MK-STYX to MK-STYX_{active mutant} and also to its active homologs MKP-1 (DUSP-1) and MKP-3 (DUSP-6).

Experimental Approach

An essential step towards elucidating the role of MK-STYX in stress response pathways is to determine its macromolecular structure. Determining the macromolecular structure of a protein is an important step towards understanding the unique relationship between structure and function in that protein^{14,43}. Knowing the structure leads to uncovering the molecular mechanisms of the protein. It also allows for the development of drugs to target the protein if it is involved in disease pathways. Traditional approaches for structure determination include: X-ray crystallography, nuclear magnetic resonance (NMR) spectroscopy, and cryo-electron microscopy (cryo-EM). These methods use different types of experimental data to determine the overall macromolecular structure of a protein. X-ray crystallography uses the data from the X-ray diffraction pattern, NMR uses the distance between atoms, and cryo-EM uses beams of electrons to form images of individual molecules⁴⁴⁻⁴⁷.

Full or partial structures have already been determined for the active homologs of MK-STYX, MKP-1⁴³ and MKP-3^{14,15}, and for the prototypical pseudophosphatase STYX⁴⁸. The structure of the catalytic domain of MKP-1 was determined using X-ray crystallography and revealed that the protein is able to bind both phosphorylated tyrosine and threonine side chains because it has a shallow active site¹⁵. Two partial structures for MKP-3 are known, that of the C-terminal catalytic domain and of the N-terminal domain^{14,43}. The structure of the N-terminal domain, also referred to as the ERK2 binding (EB) domain, of MKP-3 was determined using NMR spectroscopy¹⁴. The structure showed that binding of ERK2 is required for activation of MKP-3 because it induces a conformational change of the C-terminal catalytic domain, revealing that the two domains are functionally coupled. MKP-1 and MKP-3 are examples of how elucidating the macromolecular structure of a protein is a critical step in understanding the function of the protein and the novel mechanisms utilized to carry out its role in cellular pathways.

Materials and Methods

Protein Expression

The sequences for MK-STYX, MK-STYX_{active mutant}, and the truncated versions of MK-STYX (MK-STYX_{CH2 truncate} and MK-STYX_{DUSP truncate}), were each cloned into a pET28a+ vector containing a polyhistidine sequence (His-tag), a kanamycin resistance gene, and a T7 promoter (GenScript)⁴⁹. Competent *Escherichia coli* containing a DE3 recombinant phage, which encodes for the inducible T7 RNA polymerase, were then transformed with one of the previously mentioned plasmids and grown overnight on kanamycin treated Luria Broth (LB)-agar plates.

The next day a colony was selected from the plate and grown overnight in LB

liquid medium in a shaking incubator. On the following day, the overnight culture was used to inoculate fresh LB liquid medium, ranging in volume from 3mL to 1L. These subcultures were incubated with shaking until ready to induce. IPTG (isopropyl β -D-1-thiogalactopyranoside) was added to the cultures to induce expression of the protein of interest and then incubated with shaking at a range of temperatures and for varying durations in order to find the expression conditions that were the most favorable. The final cultures were centrifuged, and the bacterial cell pellets stored at -20°C. Protein expression and solubility were analyzed using Western Blots with primary antibodies against both MK-STYX (anti-STYXL1, Abcam ab67913) and the His-tag (anti-6x His-tag, Abcam ab18184).

Protein Purification Under Native Conditions

Purification was done using immobilized metal ion affinity chromatography (IMAC) to separate out the His-tagged protein of interest. Multiple methods were tested in order to optimize purification.

Lysis: The bacterial cell pellets were lysed using a method adapted from “Protocol 9. Preparation of cleared *E. coli* lysates under native conditions” from the 5th edition QIAexpressionist™ (QIAGEN). First the pellets were thawed on ice, then they were resuspended in lysis buffer (50mM NaH₂PO₄, 300mM NaCl, 10mM imidazole, Halt™ Protease Inhibitor Cocktail (Thermo Scientific)). Then the lysate was either sonicated or run through a high-pressure hydraulic press. The lysate was centrifuged at 10,000 x g for 20-30 min at 4°C to separate out the soluble fraction.

Fast Protein Liquid Chromatography (FPLC) Method of Purification: The soluble fraction was loaded onto a HisTrap™ HP 5mL column (Cytiva), which is prepacked with nickel (Ni²⁺) resin, and run on the ÄKTA™ pure chromatography system (Cytiva)

following “Protocol 13. FPLC purification of 6xHis-tagged proteins from *E. coli* using Ni-NTA Superflow under native conditions” from the 5th edition QIAexpressionist™ (QIAGEN).

After the HisTrap™ and FPLC method did not yield sufficient protein purity, later purification methods used cobalt resin (Co²⁺) because, while it has lower adsorption than nickel resin, it has higher specificity and so it can reduce the level of nonspecific binding⁵⁰.

Gravity-flow Method of Purification: The 2-10mL column from the Disposable Column Trial Pack (Thermo Scientific) was placed on a clamp stand in the cold room (4°C) and packed with HisPur™ Cobalt Resin (Thermo Scientific) according to the manufacturer’s protocol. Then the soluble fraction was purified according to the protocol for “Purification of His-tagged Proteins using a Gravity-flow Column” in the HisPur™ Cobalt Resin instructions (Thermo Scientific).

Batch Method of Purification: HisPur™ Cobalt Resin (Thermo Scientific, product no. 89964) was transferred to a 15mL conical tube and the manufacturer’s protocol for “Purification of His-Tagged Proteins by Batch Method” was followed.

Spin-column Method of Purification: The HisPur™ Cobalt Spin Columns, 3.0mL resin bed (Thermo Scientific, product no. 89969) were used according to the manufacturer’s protocol.

Large-scale purification: After the batch method of purification was determined to yield the best quality samples, the process was scaled up (8x) for large-scale purification. The elution fractions with the best level of purity were used for a crystal screen.

Quality Control: For each cobalt resin-based method of purification, the elution fractions were checked for protein quality and quantity using SDS-PAGE and a Bradford assay. Then a Western Blot was performed using anti-STYXL1 as the primary antibody (Abcam ab67913) to confirm the presence of MK-STYX in the sample.

Preparation of Sample for a Crystal Screen

Before the protein sample can be used for a crystal screen, it must be dialyzed to remove the imidazole and reduce the salt concentration of the sample buffer, and then be concentrated to increase the protein concentration of the sample. Depending on the volume of elution fractions, the fractions were either concentrated and then dialyzed, or dialyzed and then concentrated.

Sample Concentration: A centrifugal filter, such as the Pierce™ Protein Concentrator PES 10K MWCO, 5-20mL (Thermo Scientific), was used to concentrate the elution fractions. First the filter was rinsed with ddH₂O, 15mL of water was added to the filter and then it was spun at 3000-5000 x g for 20 minutes at 4°C. The water was discarded, and the rinse step was repeated with elution buffer. The elution buffer was then discarded and up to 15mL of elution fractions was added to the filter. It was then spun at 3000-5000 x g for 20 minutes at 4°C. The flow-through was removed and more of the remaining elution fractions were added to the filter. It was then spun at 3000-5000 x g for up to 20 minutes at 4°C. This process was repeated until all of the elution fractions had been added and until the sample was concentrated to the desired final volume and/or protein concentration.

Sample Dialysis: To dialyze the sample, the Slide-A-Lyzer™ (Thermo Scientific) dialysis system was used, which has kits that cover a variety of sample volumes to accommodate both small- and large-scale purifications. First, the Slide-A-Lyzer™ membrane was hydrated with dialysis buffer (Tris buffer with 150mM NaCl). The sample was loaded into the Slide-A-Lyzer™, and any excess air was removed. The Slide-A-Lyzer™ was floated in dialysis buffer for at least 2 hours at 4°C. The old dialysis buffer was replaced with fresh buffer and left for at least another 2 hours at 4°C, then this dialysis buffer was replaced with fresh buffer and left overnight at

4°C. The next day, the sample was removed and kept on ice or stored at 4°C.

Crystal Screen

Using a Crystal Gryphon robot (Art Robbins Instruments), the protein sample was mixed with seven different commercially available sets of crystallization conditions and then crystallization drops were dispensed onto seven different 96-well INTELLI-PLATES⁵¹. The Minstrel DT UV Protein Crystal Imaging system (Rigaku) takes pictures of the crystallization drops on day 0, day 1, and every subsequent 3 days.

Results

Figure 2 shows the SDS-PAGE results of selected elution fractions from purification using the HisTrap™ column (Cytiva) for FPLC, along with a molecular weight (MW) marker. There were more than ten different proteins in each elution fraction. The FPLC and HisTrap™ column combination was not successful at isolating MK-STYX to an adequate purity needed to proceed to a crystal screen.

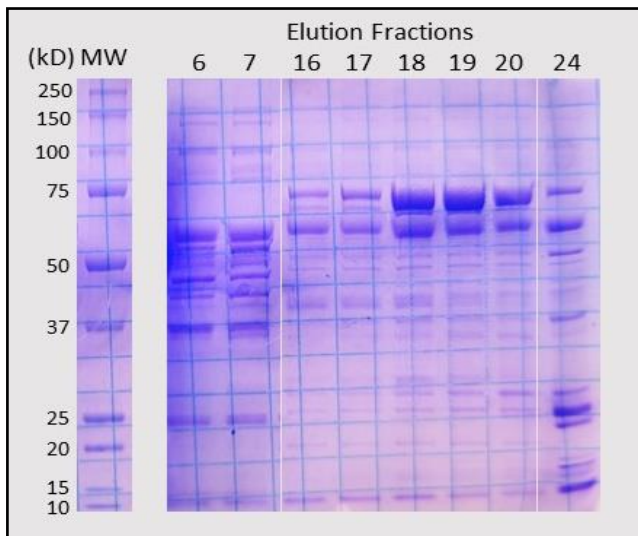


Figure 2: Results of SDS-PAGE after purification using the HisTrap™ column (Cytiva). Coomassie stained gel shows a MW marker and some of the elution fractions, which are named in sequential order based on when they were eluted.

Figure 3 shows the comparative results of multiple purification experiments done using cobalt resin and using manual

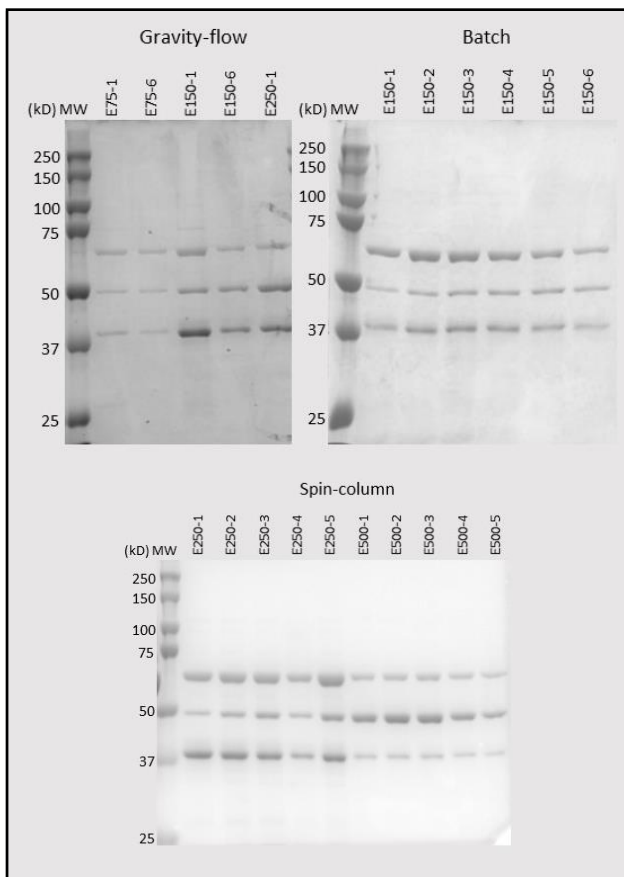


Figure 3: Results of three different purification methods using cobalt resin. Each coomassie stained gel shows the elution fractions obtained from three different methods of purification (gravity-flow, batch and spin-column). The elution fractions (E) are named based on the concentration of imidazole in the elution buffer (75mM-500mM) and the sequential order in which they were eluted (1-6). Images taken with the Invitrogen iBright Imaging System.

purification methods (gravity-flow, batch, and spin-column). There were only minimal differences in the quality of elution fractions between the different methods, and between different elution buffer imidazole concentrations. The batch purification method was determined to be the best option due to its speed, compared to the gravity-flow method, and because of its ability to easily be scaled up for larger scale purifications, compared to the spin-column method.

Figure 4 shows the results of a Western Blot performed on the elution fractions of a large-scale batch method purification. MK-STYX (~37 kD) is shown in white after being probed with the primary antibody anti-STYXL1, probed with the secondary antibody anti-mouse IgG (immunoglobulin G), HRP

(horseradish peroxidase) conjugate, incubated with ECL (enhanced chemiluminescence) Western Blotting substrate, and imaged using the Invitrogen iBright Imaging System (Thermo Scientific). This confirms that the protein that was purified was MK-STYX.

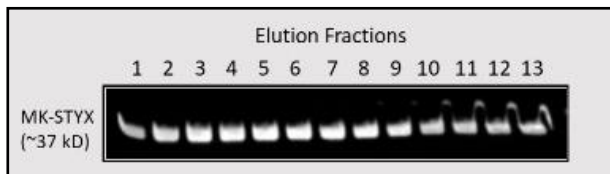


Figure 4: Confirmation of MK-STYX in the elution fractions from a large-scale purification. Shows the elution fractions obtained from a large-scale batch method purification with the ECL detection in white. The primary antibody used was STYXL1 and the band was ~37 kD, which was the expected MW of MK-STYX. Imaged using the Invitrogen iBright Imaging System

Figure 5 shows selected crystallization drops from a crystal screen as imaged by the Minstrel DT UV Protein Crystal Imaging system (Rigaku) immediately after they were dispensed by the Crystal Gryphon robot (Art Robbins Instruments). This demonstrates some of the possible visual characteristics the drops can have, such as clear (upper-left drop) or with different levels of precipitation (precipitation increases in the drops in a clockwise direction).

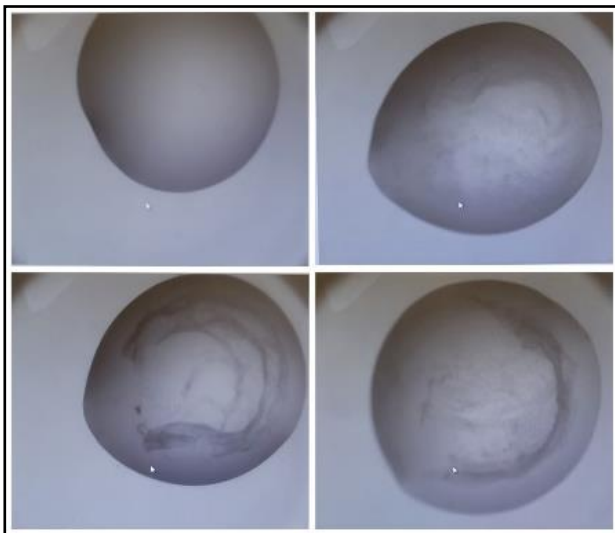


Figure 5: Pictures of crystallization drops from a crystal screen. A selection of drops that show different levels of precipitation at day 0. Imaged by the Minstrel DT UV Protein Crystal Imaging system.

Discussion

After finding that the FPLC elution fractions were not the level of purity needed to

obtain a protein crystal, the purification process was reevaluated. It was determined that a manual method of purification would be better suited to MK-STYX. In addition to switching from an automated IMAC method to a manual IMAC method, nickel-based resin was swapped for cobalt-based resin to decrease the number of non-specific bands that were present in the previous elution fractions.

Using three different types of small-scale manual purification methods allowed for optimization of the large-scale purification process, by pointing out the pros and cons of each method and providing insight into whether the methods could be scaled up. The gravity-flow method had logistical issues due to the fact that it needed to be done in a shared cold room, where space was an issue. This method also took much longer since the wash and elution buffers had to flow through the resin at a dropwise pace. The spin-column method led to lower protein yield, as determined by a Bradford assay, possibly due to the fact that the resin became dried out after each spin. Another issue with the spin-column method was that it was not feasible to scale up, since the largest commercially available column volume was already the size being used. In conclusion, the batch method of purification was determined to be the best option since it had about the same level of non-specific binding as the other methods, it could easily be scaled up, and it did not pose any major logistical issues.

The process of obtaining a crystal structure consists of numerous steps: form a protein crystal, direct an X-ray beam at the crystal in order to make a diffraction pattern, use that information to generate an electron density map, and then determine the atomic model^{52,53}. However, before any of those steps can begin, there must first be a suitable protein crystal available. Obtaining a suitable protein crystal can be a long and sometimes tedious process while the experimental conditions are optimized to the protein of interest. At the time

of paper submission, no crystals have yet been obtained from the current crystal screen. As it can take some time for crystals to form, the screen is still ongoing and a crystal may form later. In the meantime, we are preparing to start a new crystal screen to test out more crystallization conditions. We will continue to work towards determining the crystal structure of MK-STYX due to the pressing need to elucidate the macromolecular structure of MK-STYX in order to understand the function of such a unique protein.

Previously, computational approaches were used to provide insight into how the structure of MK-STYX may influence the binding capabilities of the protein²⁴. A mutagenesis study on a computer-predicted model of MK-STYX showed that when the KIM is mutated to restore consecutive arginines, in the same positions as its active homolog MKP-3, it changes the shape and volume of the associated binding pocket in MK-STYX. Since the KIM is a conserved sequence in MKPs and regulates their specificity in signaling pathways, this may explain why MK-STYX does not function as a typical MKP^{13,16,23,24,28}. MK-STYX could instead be using a novel mechanism to regulate critical signaling pathways, such as stress response. If this binding site is confirmed by crystallography, it would be an important step in developing drugs that target MK-STYX.

Once the macromolecular structure of MK-STYX is obtained, it will allow us to understand the relationship between the structure and the function of MK-STYX. Additionally, it will uncover how the atypical domains of MK-STYX are linked to the mode of action that allows MK-STYX to regulate cellular stress response pathways, and identify the mechanisms utilized by MK-STYX, beyond those used by its active homologs. MK-STYX continues to be linked to an increasing number of signaling pathways and human diseases^{24,32}. Which is why determining the macromolecular structure of MK-STYX is

such a critical step towards uncovering the molecular mechanisms that define the role of MK-STYX in the cell. Until this is known, it will not be possible to fully understand these pathways or to find ways to target them in order to treat the associated diseases.

Acknowledgments

The author wishes to thank Dr. Shantá D. Hinton for her guidance and support. The author also wishes to thank Lynn Zavada for her contributions to this project. Additionally, the author would like to thank Dr. Martin Safo and Dr. Faik Musayev of the VCU School of Pharmacy's Institute for Structural Biology, Drug Discovery and Development. The author would like to give special thanks to the Virginia Space Grant Consortium for their financial support. This work was also supported by the National Science Foundation Grant MCB1909316 to S.D.H.

References

- (1) Hinton, S. D. The Role of Pseudophosphatases as Signaling Regulators. *Biochimica et Biophysica Acta (BBA) - Molecular Cell Research* **2019**, *1866* (1), 167–174. <https://doi.org/10.1016/j.bbamcr.2018.07.021>.
- (2) Protein Kinases and Phosphatases: The Yin and Yang of Protein Phosphorylation and Signaling. *Cell* **1995**, *80* (2), 225–236. [https://doi.org/10.1016/0092-8674\(95\)90405-0](https://doi.org/10.1016/0092-8674(95)90405-0).
- (3) Tonks, N. K. Protein Tyrosine Phosphatases – from Housekeeping Enzymes to Master Regulators of Signal Transduction. *The FEBS Journal* **2013**, 346–378. [https://doi.org/10.1111/febs.12077@10.1002/\(ISSN\)1742-4658\(CAT\)FreeReviewContent\(VI\)Reviews1213](https://doi.org/10.1111/febs.12077@10.1002/(ISSN)1742-4658(CAT)FreeReviewContent(VI)Reviews1213).
- (4) Murphy, J. M.; Farhan, H.; Evers, P. A. Bio-Zombie: The Rise of Pseudoenzymes in Biology. *Biochem Soc Trans* **2017**, *45* (2), 537–544. <https://doi.org/10.1042/BST20160400>.
- (5) Todd, A. E.; Orengo, C. A.; Thornton, J. M. Sequence and Structural Differences between Enzyme and Nonenzyme Homologs. *Structure* **2002**, *10* (10), 1435–1451. [https://doi.org/10.1016/S0969-2126\(02\)00861-4](https://doi.org/10.1016/S0969-2126(02)00861-4).
- (6) Murphy, J. M.; Mace, P. D.; Evers, P. A. Live and Let Die: Insights into Pseudoenzyme Mechanisms from Structure. *Current Opinion in Structural Biology* **2017**, *47*, 95–104. <https://doi.org/10.1016/j.sbi.2017.07.004>.
- (7) Reiterer, V.; Evers, P. A.; Farhan, H. Day of the Dead: Pseudokinases and Pseudophosphatases in Physiology and Disease. *Trends in Cell Biology* **2014**, *24* (9), 489–505. <https://doi.org/10.1016/j.tcb.2014.03.008>.
- (8) Reiterer, V.; Pawłowski, K.; Desrochers, G.; Pause, A.; Sharpe, H. J.; Farhan, H. The Dead Phosphatases Society: A Review of the Emerging Roles of Pseudophosphatases. *The FEBS Journal* **2020**, *287* (19), 4198–4220. <https://doi.org/10.1111/febs.15431>.
- (9) Tonks, N. K. Pseudophosphatases: Grab and Hold On. *Cell* **2009**, *139* (3), 464–465. <https://doi.org/10.1016/j.cell.2009.10.008>.

- (10) Hinton, S. D.; Myers, M. P.; Roggero, V. R.; Allison, L. A.; Tonks, N. K. The Pseudophosphatase MK-STYX Interacts with G3BP and Decreases Stress Granule Formation. *Biochem J* **2010**, *427* (Pt 3), 349–357. <https://doi.org/10.1042/BJ20091383>.
- (11) Hinton, S. D. Pseudophosphatase MK-STYX: The Atypical Member of the MAP Kinase Phosphatases. *The FEBS Journal* **2020**, *287* (19), 4221–4231. <https://doi.org/10.1111/febs.15426>.
- (12) Niemi, N. M.; MacKeigan, J. P. MK-STYX. In *Encyclopedia of Signaling Molecules*; Choi, S., Ed.; Springer: New York, NY, 2012; pp 1089–1093. https://doi.org/10.1007/978-1-4419-0461-4_205.
- (13) Caunt, C. J.; Keyse, S. M. Dual-Specificity MAP Kinase Phosphatases (MKPs). *The FEBS Journal* **2013**, *280* (2), 489–504. <https://doi.org/10.1111/j.1742-4658.2012.08716.x>.
- (14) Farooq, A.; Chaturvedi, G.; Mujtaba, S.; Plotnikova, O.; Zeng, L.; Dhalluin, C.; Ashton, R.; Zhou, M.-M. Solution Structure of ERK2 Binding Domain of MAPK Phosphatase MKP-3: Structural Insights into MKP-3 Activation by ERK2. *Molecular Cell* **2001**, *7* (2), 387–399. [https://doi.org/10.1016/S1097-2765\(01\)00186-1](https://doi.org/10.1016/S1097-2765(01)00186-1).
- (15) Stewart, A. E.; Dowd, S.; Keyse, S. M.; McDonald, N. Q. Crystal Structure of the MAPK Phosphatase Pyst1 Catalytic Domain and Implications for Regulated Activation. *Nat. Struct. Biol.* **1999**, *6* (2), 174–181. <https://doi.org/10.1038/5861>.
- (16) Nichols, A.; Camps, M.; Gillieron, C.; Chabert, C.; Brunet, A.; Wilsbacher, J.; Cobb, M.; Pouyssegur, J.; Shaw, J. P.; Arkinstall, S. Substrate Recognition Domains within Extracellular Signal-Regulated Kinase Mediate Binding and Catalytic Activation of Mitogen-Activated Protein Kinase Phosphatase-3. *J. Biol. Chem.* **2000**, *275* (32), 24613–24621. <https://doi.org/10.1074/jbc.M001515200>.
- (17) Tonks, N. K. Protein Tyrosine Phosphatases: From Genes, to Function, to Disease. *Nat. Rev. Mol. Cell Biol.* **2006**, *7* (11), 833–846. <https://doi.org/10.1038/nrm2039>.
- (18) Tonks, N. K. Special Issue: Protein Phosphatases: From Molecules to Networks. *The FEBS Journal* **2013**, *280* (2), 323–323. <https://doi.org/10.1111/febs.12098>.
- (19) Tonks, N. K.; Neel, B. G. Combinatorial Control of the Specificity of Protein Tyrosine Phosphatases. *Current Opinion in Cell Biology* **2001**, *13* (2), 182–195. [https://doi.org/10.1016/S0955-0674\(00\)00196-4](https://doi.org/10.1016/S0955-0674(00)00196-4).
- (20) Reiterer, V.; Pawlowski, K.; Farhan, H. STYX: A Versatile Pseudophosphatase. *Biochem Soc Trans* **2017**, *45* (2), 449–456. <https://doi.org/10.1042/BST20160279>.
- (21) Wishart, M. J.; Dixon, J. E. Gathering STYX: Phosphatase-like Form Predicts Functions for Unique Protein-Interaction Domains. *Trends in Biochemical Sciences* **1998**, *23* (8), 301–306. [https://doi.org/10.1016/S0968-0004\(98\)01241-9](https://doi.org/10.1016/S0968-0004(98)01241-9).
- (22) Wishart, M. J.; Denu, J. M.; Williams, J. A.; Dixon, J. E. A Single Mutation Converts a Novel Phosphotyrosine Binding Domain into a Dual-Specificity Phosphatase. *J. Biol. Chem.* **1995**, *270* (45), 26782–26785. <https://doi.org/10.1074/jbc.270.45.26782>.
- (23) Peti, W.; Page, R. Molecular Basis of MAP Kinase Regulation. *Protein Sci.* **2013**, *22* (12), 1698–1710. <https://doi.org/10.1002/pro.2374>.
- (24) Hepworth, E. M. W.; Hinton, S. D. Pseudophosphatases as Regulators of MAPK Signaling. *Int J Mol Sci* **2021**, *22* (22). <https://doi.org/10.3390/ijms22212595>.
- (25) Niemi, N. M.; Lanning, N. J.; Klomp, J. A.; Tait, S. W.; Xu, Y.; Dykema, K. J.; Murphy, L. O.; Gaither, L. A.; Xu, H. E.; Furge, K. A.; et al. MK-STYX, a Catalytically Inactive Phosphatase Regulating Mitochondrially Dependent Apoptosis. *Molecular and Cellular Biology* **2011**, *31* (7), 1357–1368. <https://doi.org/10.1128/MCB.00788-10>.
- (26) Flowers, B. M.; Rusnak, L. E.; Wong, K. E.; Banks, D. A.; Muniyikwa, M. R.; McFarland, A. G.; Hinton, S. D. The Pseudophosphatase MK-STYX Induces Neurite-Like Outgrowths in PC12 Cells. *PLoS One* **2014**, *9* (12). <https://doi.org/10.1371/journal.pone.0114535>.
- (27) Dahal, A.; Hinton, S. D. Antagonistic Roles for STYX Pseudophosphatases in Neurite Outgrowth. *Biochemical Society Transactions* **2017**, *45* (2), 381–387. <https://doi.org/10.1042/BST20160273>.
- (28) Owens, D. M.; Keyse, S. M. Differential Regulation of MAP Kinase Signalling by Dual-Specificity Protein Phosphatases. *Oncogene* **2007**, *26* (22), 3203–3213. <https://doi.org/10.1038/sj.onc.1210412>.
- (29) Niemi, N. M.; Sacoman, J. L.; Westrate, L. M.; Gaither, L. A.; Lanning, N. J.; Martin, K. R.; MacKeigan, J. P. The Pseudophosphatase MK-STYX Physically and Genetically Interacts with the Mitochondrial Phosphatase PTPMT1. *PLoS One; San Francisco* **2014**, *9* (4), e93896. <http://dx.doi.org/10.1371/journal.pone.0093896>.
- (30) Tomar, V. S.; Baral, T. K.; Nagavelu, K.; Somasundaram, K. Serine/Threonine/Tyrosine-Interacting-like Protein 1 (STYXL1), a Pseudo Phosphatase, Promotes Oncogenesis in Glioma. *Biochemical and Biophysical Research Communications* **2019**, *515* (1), 241–247. <https://doi.org/10.1016/j.bbrc.2019.05.093>.
- (31) J. Z. Wu; N Jiang; J. M. Lin; X. Liu. STYXL1 Promotes Malignant Progression of Hepatocellular Carcinoma via Downregulating CELF2 through the PI3K/Akt Pathway. *European Review* **2020**, *24* (6), 2977–2985. https://doi.org/10.26355/eurrev_202003_20662.
- (32) Mattei, A. M.; Smailys, J. D.; Hepworth, E. M. W.; Hinton, S. D. The Roles of Pseudophosphatases in Disease. *Int J Mol Sci* **2021**, *22* (13). <https://doi.org/10.3390/ijms22136924>.
- (33) Banks, D. A.; Dahal, A.; McFarland, A. G.; Flowers, B. M.; Stephens, C. A.; Swack, B.; Gugssa, A.; Anderson, W. A.; Hinton, S. D. MK-STYX Alters the Morphology of Primary Neurons, and Outgrowths in MK-STYX Overexpressing PC-12 Cells Develop a Neuronal Phenotype. *Front Mol Biosci* **2017**, *4*. <https://doi.org/10.3389/fmolb.2017.00076>.
- (34) Youn, J.-Y.; Dyakov, B. J. A.; Zhang, J.; Knight, J. D. R.; Vernon, R. M.; Forman-Kay, J. D.; Gingras, A.-C. Properties of Stress Granule and P-Body Proteomes. *Molecular Cell* **2019**, *76* (2), 286–294. <https://doi.org/10.1016/j.molcel.2019.09.014>.
- (35) Protter, D. S. W.; Parker, R. Principles and Properties of Stress Granules. *Trends in Cell Biology* **2016**, *26* (9), 668–679. <https://doi.org/10.1016/j.tcb.2016.05.004>.
- (36) Barr, J. E.; Muniyikwa, M. R.; Frazier, E. A.; Hinton, S. D. The Pseudophosphatase MK-STYX Inhibits Stress Granule Assembly Independently of Ser149 Phosphorylation of G3BP-1. *The FEBS Journal* **2013**, *280* (1), 273–284. <https://doi.org/10.1111/febs.12068>.
- (37) Guillén-Boixet, J.; Kopach, A.; Holehouse, A. S.; Wittmann, S.; Jahnel, M.; Schlübler, R.; Kim, K.; Trussina, I. R. E. A.; Wang, J.; Mateju, D.; et al. RNA-Induced Conformational Switching and Clustering of G3BP Drive Stress Granule Assembly by Condensation. *Cell* **2020**, *181* (2), 346–361.e17. <https://doi.org/10.1016/j.cell.2020.03.049>.
- (38) Nemoto, S.; Ohnuki, S.; Abe, F.; Ohya, Y. Simulated Microgravity Triggers Characteristic Morphology and Stress Response in *Saccharomyces cerevisiae*. *Yeast* **2019**, *36* (2), 85–97. <https://doi.org/10.1002/yea.3361>.
- (39) Graebe, A.; Schuck, E. L.; Lensing, P.; Putcha, L.; Derendorf, H. Physiological, Pharmacokinetic, and Pharmacodynamic Changes in Space. *The Journal of Clinical Pharmacology* **2004**, *44* (8), 837–853. <https://doi.org/10.1177/0091270004267193>.
- (40) Qu, L.; Chen, H.; Liu, X.; Bi, L.; Xiong, J.; Mao, Z.; Li, Y. Protective Effects of Flavonoids Against Oxidative Stress Induced by Simulated Microgravity in SH-SY5Y Cells. *Neurochem Res* **2010**, *35* (9), 1445–1454. <https://doi.org/10.1007/s11064-010-0205-4>.

- (41) Zhao, L.; Rui, Q.; Wang, D. Molecular Basis for Oxidative Stress Induced by Simulated Microgravity in Nematode *Caenorhabditis Elegans*. *Science of The Total Environment* **2017**, *607–608*, 1381–1390. <https://doi.org/10.1016/j.scitotenv.2017.07.088>.
- (42) Hinton, S. D. Analyzing Pseudophosphatase Function. In *Protein Tyrosine Phosphatases: Methods and Protocols*; Pulido, R., Ed.; Methods in Molecular Biology; Springer: New York, NY, 2016; pp 139–153. https://doi.org/10.1007/978-1-4939-3746-2_9.
- (43) Gumpena, R.; Lountos, G. T.; Raran-Kurussi, S.; Tropea, J. E.; Cherry, S.; Waugh, D. S. Crystal Structure of the Human Dual Specificity Phosphatase 1 Catalytic Domain. *Protein Sci.* **2018**, *27* (2), 561–567. <https://doi.org/10.1002/pro.3328>.
- (44) Callaway, E. Revolutionary Cryo-EM Is Taking over Structural Biology. *Nature* **2020**, *578*, 201–201. <https://doi.org/10.1038/d41586-020-00341-9>.
- (45) Liu, H.-L.; Hsu, J.-P. Recent Developments in Structural Proteomics for Protein Structure Determination. *PROTEOMICS* **2005**, *5* (8), 2056–2068. <https://doi.org/10.1002/pmic.200401104>.
- (46) Berman, H. M.; Westbrook, J.; Feng, Z.; Gilliland, G.; Bhat, T. N.; Weissig, H.; Shindyalov, I. N.; Bourne, P. E. The Protein Data Bank. *Nucleic Acids Res* **2000**, *28* (1), 235–242. <https://doi.org/10.1093/nar/28.1.235>.
- (47) Wlodawer, A.; Minor, W.; Dauter, Z.; Jaskolski, M. Protein Crystallography for Non-Crystallographers, or How to Get the Best (but Not More) from Published Macromolecular Structures. *FEBS J* **2008**, *275* (1), 1–21. <https://doi.org/10.1111/j.1742-4658.2007.06178.x>.
- (48) Almo, S. C.; Bonanno, J. B.; Sauder, J. M.; Emtage, S.; Dilorenzo, T. P.; Malashkevich, V.; Wasserman, S. R.; Swaminathan, S.; Eswaramoorthy, S.; Agarwal, R.; et al. Structural Genomics of Protein Phosphatases. *J Struct Funct Genomics* **2007**, *8* (2), 121–140. <https://doi.org/10.1007/s10969-007-9036-1>.
- (49) Wise, M. C. ISB3D X-Ray Crystallography Facility. 5.
- (50) Takara Bio. How to Choose the Right His-Tagged Purification Resin. <https://www.takarabio.com/about/bioview-blog/tips-and-troubleshooting/choosing-a-his-tagged-purification-resin>, **2019**.
- (51) Belvin, B. R.; Musayev, F. N.; Burgner, J.; Scarsdale, J. N.; Escalante, C. R.; Lewis, J. P. Nitrosative Stress Sensing in *Porphyromonas Gingivalis*: Structure of and Heme Binding by the Transcriptional Regulator HcpR. *Acta Cryst D* **2019**, *75* (4), 437–450. <https://doi.org/10.1107/S205979831900264X>.
- (52) Rhodes, G. *Crystallography Made Crystal Clear: A Guide for Users of Macromolecular Models*; Elsevier Science & Technology: Burlington, UNITED STATES, **2006**.
- (53) Petsko, G. A. *Protein Structure and Function*; Primers in biology; Oxford University Press; Distributed inside North America by Sinauer Associates: Oxford [England]; New York: Sunderland, MA, **2009**.